ELSEVIER

International Journal of Adhesion & Adhesives 18 (1998) 199–213

Adhesion & Adhesives

Static and fatigue crack growth of epoxy adhesives and fractal dimensions

Kimiyoshi Naito[a], Toru Fujii[b,*]

[a]DOSHISHA University, College of Engineering, Japan
[b]Department of Mechanical Engineering and Systems, Doshisha University, Kyotanabe-shi 610-0321, Japan

Accepted 8 December 1997

Abstract

Fractured surfaces of epoxy adhesives under mode I static and fatigue (cyclic) loading have fractal characteristics. The effects of rubber modification, adhesive thickness and cross-head speed (static only) on both static and fatigue fracture surfaces of epoxy adhesives were examined using fractals.

Under static loading, the fractal dimension becomes high due to rubber modification. It is related to the static crack growth properties for both unmodified and rubber-modified adhesives. The following equation gives the relationship between the observed crack extension resistance, G_I and the fractal dimension, D:

$$\log G_I = \alpha_1 \cdot D + \beta_1,$$

where α_1 and β_1 are experimental constants. Regardless of whether adhesives contain rubber particles or not, the fractal dimension is not affected by adhesive thickness and cross-head speed.

Under fatigue loading, the fractal dimension of the fractured surfaces becomes high due to rubber modification under the same energy release rate range, ΔG_I when ΔG_I is higher than 100 J/m^2. The fractal dimension decreases with an increase in the fatigue crack growth rate, da/dN. A relationship is given by the following equation between a surface 'fatigue working' parameter for the crack, $S(= da/dN \cdot \Delta G_I)$ and the fractal dimension for unmodified and rubber modified adhesives:

$$\log S = \log\left(\frac{da}{dN} \cdot \Delta G_1\right) = \alpha_5 \cdot D + \beta_5,$$

where α_5 and β_5 are experimental constants. Whether the adhesives contain rubber particles or not, the fractal dimension as well as the $da/dN - \Delta G_I$ relation is little affected by adhesive thickness.

Key words: A. toughened adhesives; B. steels; C. fracture mechanics; D. fracture

1. Introduction

Epoxy adhesives have been modified by using various methods to improve their fracture toughness [1–3]. In studies on the fracture toughness of adhesively-bonded joints, fracture surfaces are always examined to distinguish the failure characteristics by using a SEM [4–6]. Such surfaces are thought to have inherent properties in response to the failure process of the adhesives, namely, the fractured surface could be related to the fracture toughness and durability of adhesive-bonded joints. For example, the fractured surface of rubber-modified adhesives is more complex than that for unmodified adhesives [7]. A toughening mechanism for rubber-modified adhesives has also been examined with fracture surface analysis. Many workers studied the toughening and fracture surfaces of rubber-modified adhesives [8,9]. However, in the absence of a theoretical basis for analysis and experimental methodology, much of the surface information is often ignored. Early investigators simply characterized the geometry of fracture surfaces using terms such

*Corresponding author.

0143-7496/98/$19.00
PII: S0143-7496(97)00004-9

as 'complex' or 'rough', while the roughness defined by national standards such as JIS [10] (Japanese Industrial Standard), BS, ASTM or ISO [11] is sometimes used to evaluate surface geometry quantitatively. However, we believe that such standards are insufficient to distinguish the differences between fractured surfaces of adhesives. A more meaningful quantitative characterization of fractured surfaces is very desirable for estimating the fracture mechanisms in adhesive-bonded joints.

The authors have revealed that the fractured surfaces of epoxy adhesives under both static and fatigue loadings have fractal characteristics [12]. We also established from the physical point of view using the linear finite-element analysis that the fractal dimension of fractured surfaces can be related to the energy release rate. Therefore, we believe that the effects of various factors on both static crack growth properties of adhesive-bonded joints and fractured surfaces of epoxy adhesives can be clearly established using the fractal dimension.

In the present study, we investigate the static and fatigue fracture surfaces of epoxy adhesives evaluated quantitatively by using fractals. We also examine the effects of rubber modification and adhesive thickness on static and fatigue fracture surfaces of epoxy adhesives by using fractals. Mode I tests were conducted using double cantilever beam (DCB) specimens fabricated with unmodified and rubber-modified adhesives.

2. Experiment

2.1. Specimens

DCB specimens were employed, with mode I loads being applied to the specimens both statically and cyclically. The specimen dimensions are shown in Fig. 1. An epoxy adhesive, Epikote 828 was used in this investigation. Three types of adhesive were tested: an unmodified epoxy and two CNBR (cross-linked acrylonitrile–butadiene rubber (NBR-COOH)) modified epoxies (2.8 and 5.5% modified, by weight). In this rubber modification method, sub-micron rubber particles, 70–200 nm in diameter, have been mixed into an epoxy resin (not hardener) before the resin and the hardener are mixed to consolidate [13]. Therefore, the epoxy resin can contain rubber particles whose diameters are almost constant after curing. Relatively high-strength carbon steel was used for the adherends. The surfaces of the adherends were abraded with sandpaper and solvent cleaned. Two PTFE films were inserted between two adherends in order to control adhesive thickness, $t(= 0.1,\ 0.3,\ 0.5$ mm). The adhesives were cured according to the manufacturer's recommended procedure. All the specimens were kept in a chamber at $23 \pm 3^{\circ}$C and $65 \pm 5\%$ relative humidity for at least one week before testing. All the tests were conducted under the laboratory environment at room temperature.

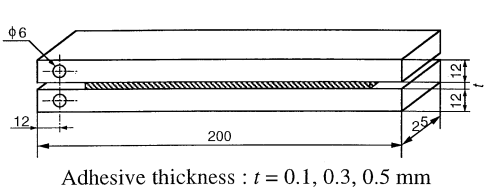

Fig. 1. Dimensions of the double cantilever beam specimen.

2.2. Static tests

All tests on the DCB specimens were performed using an Instron testing machine. The specimen, having a naturally shaped crack from an artificial pre-crack tip, was set in the testing machine using a jig. The pin connecting the DCB specimen and the tensile jig was pulled downwards until a stable crack was formed. Once stable crack growth was observed, the cross-head was stopped and held for 2 min. When the cross-head was held, the crack gradually grew and the observed load decreased. Then, the load was removed to estimate the compliance of the DCB specimen. Similar loading–unloading procedures were conducted up to final separation of the specimen. In this study, four types of cross-head speeds, v ($= 0.01, 0.1, 1, 10$ mm min^{-1}) were tested. Displacement between the loading points was measured using an extensometer. Crack length in the adhesive layer was measured intermittently using a microscope/TV system to check the crack length estimated by the compliance. The energy release rate, G_{I} was calculated by the compliance method.

2.3. Fatigue tests

Fatigue tests were conducted using a servohydraulic testing machine at a frequency of 2 Hz under cyclic loading with constant amplitude. The waveform of the cyclic load was triangular. The load ratio R between the minimum and maximum loads was 0.1. We monitored crack length, applied load and displacement continuously during the test. Crack length in the adhesive layer was also estimated from the observed compliance of the DCB specimen. The location of the crack tip was intermittently observed using the microscope/TV system to check the crack length estimated by the compliance.

2.4. Observation of fractured surfaces and measurement of fractal dimension

Fig. 2 shows the location for observation of the fracture surfaces: (a) shows the static fracture surface and; (b) shows the fatigue fracture surface. The observed area was in the center of the fracture surface and parallel to the crack growth direction. The geometry of the fracture surface was traced using a laser scanning microscope

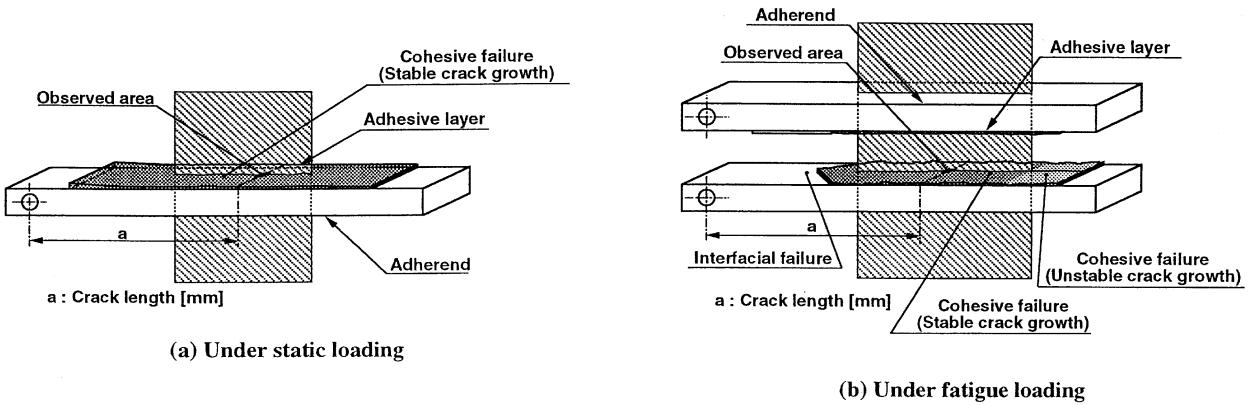

Fig. 2. Locations for fracture surface examination.

(Lasertec Corp., 1LM21). Then, the curve representing surface roughness was obtained.

The laser scanning microscope digitizes the surface topology of the failed specimen by first dividing the surface traces into 1024 equal parts in the longitudinal direction and then converting the depth of the surface from analogue to digital form. Object lenses having different magnification can be attached to the microscope, while its spatial resolution in the field of view are constant for all lenses. Along the x-axis (in the longitudinal direction), the resolution is 1024, while the resolution in depth is 256. Therefore, the surface topology can be measured in more detail when the higher magnification lens is used.

The adhesive thickness was changed from $t = 0.1$ to 0.5 mm in this study. When the adhesive thickness is 0.1 mm, the roughness (depth) of the fractured surface must be smaller than 0.1 mm. We considered that the observed distance in the longitudinal direction should approximately correspond to the adhesive thickness in order to estimate the fractal dimension of the fracture surface. When the fatigue test is conducted under cyclic loading at constant amplitude, the energy release rate changes with respect to crack length. When we try to estimate the fractal dimension of the fracture surface, it must be derivable that the energy release rate within the observed distance is almost constant; the change in energy release rate is therefore small. Therefore, we specified in the present work that the change in the energy release rate within the observed area is below 0.5%. Based on the above considerations, the $\times 50$ object lens was used and the observed distance was 0.1 mm in this study. As some data for synchronized signals are contained in the digital data for surface profiles coming from the laser scanning microscope, almost half the data (500) for each fractured surface trace will be utilized. The basic length for estimating the fractal is 0.05 mm. A resolution for measuring the surface profiles is 0.1 μm.

The fractal dimension of a curve representing the surface roughness of the failed specimen is calculated using the box counting method which we used previously [12]. If the fractured surface has fractal characteristics, there is a relationship given by the following equation between the number of boxes (squares), $N(r)$ and the side length of the box, r.

$$N(r) \propto r^{-D} \tag{1}$$

Taking the logarithm of both sides of the above equation gives

$$\log N(r) = \log C - D \log r, \tag{2}$$

where C is an arbitrary constant and D is the fractal dimension for the curve. D takes a value in the range $1 \leqslant D \leqslant 2$.

3. Results and discussion

The specimens fabricated using the epoxy adhesives failed either in a cohesive or an interfacial manner. The fractured surfaces of epoxy adhesives changed due to the test conditions.

Under static loading, the specimens bonded with the rubber-modified adhesives mostly failed cohesively as shown in Fig. 2(a). Even the specimens bonded with the unmodified adhesive mostly failed cohesively, although partial interfacial failure may have occurred. SEM micrographs of higher magnification did not reveal crack propagation within the rubber particles. Thus, rubber cavitation did not occur due to delamination. When specimens failed interfacially for the unmodified adhesive, the fractured surface was very smooth and the fracture toughness was smaller than that of the specimens which had failed cohesively. The smooth surface also had fractal characteristics with a fractal dimension of almost 1.0.

Under fatigue loading, the specimens bonded with the unmodified and rubber-modified adhesives mostly failed in the interfacial manner at low fatigue crack growth rate, as shown in Fig. 2b. When the specimens failed in the interfacial manner, the fractured surfaces were very

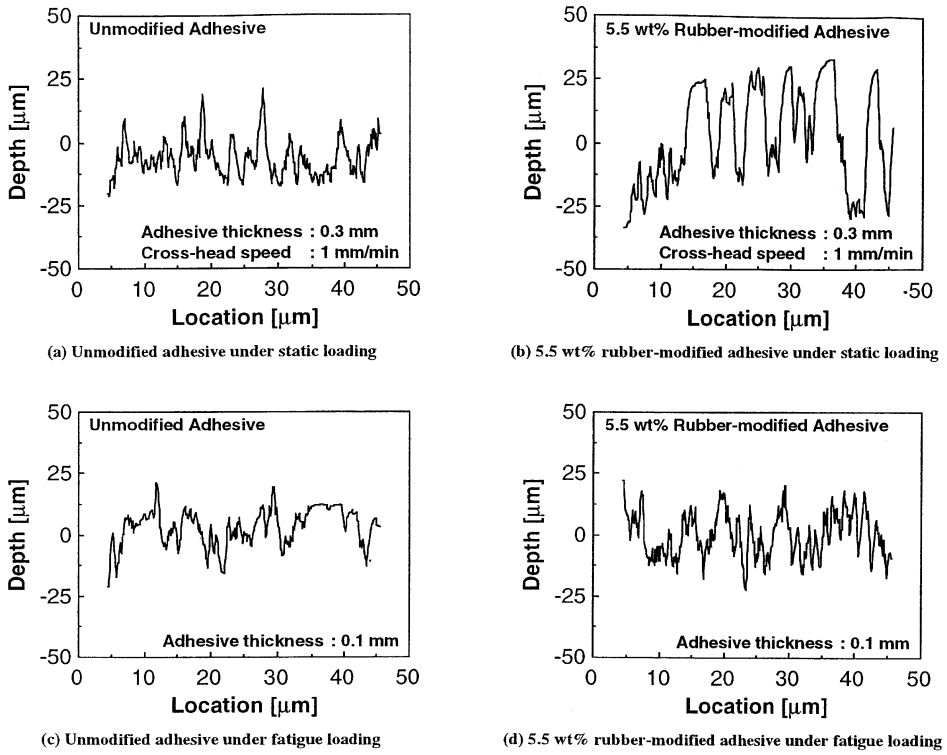

Fig. 3. Surface traces of fracture surfaces. (Unmodified and 5.5 wt% rubber-modified adhesives).

smooth and almost reflected the original surfaces of the adherends, similar to the case when the specimens failed interfacially under static loading. With an increase in the range of the energy release rate fatigue crack growth rate, cohesive failure occurred partially in the center of the adherend and spread over the width direction of the specimen. In this study, we focus on fracture surfaces caused by cohesive failure all over the width direction. Fractured surfaces caused by interfacial failure and interfacial-cohesive mixed failure were not studied.

The roughness of static and fatigue fracture surfaces measured using the laser scanning microscope are shown in Fig. 3a–d. Differences between surface characteristics of the two types of adhesives are well distinguishable.

Fig. 4a–d shows the relationship between the number of boxes, $N(r)$ and the side length of the box, r. Fig. 4 corresponds to Fig. 3. The relationship between $N(r)$ and r can be represented by a straight line having a negative slope in the log–log scaled figures. Fractal dimensions were also calculated at many locations other than the center portion. The results using the box-counting method fitted well to Eq. (1). Thus, it can be said that both static and fatigue fractured surfaces have fractal characteristics.

In order to examine the variation of the estimated fractal dimension due to a change of measuring conditions, the fractured surfaces under both static and fatigue loadings were digitally traced using object lenses having different magnifications ($\times 10$, $\times 20$, $\times 40$, $\times 50$, $\times 100$). The traces are shown in Fig. 5.[1] As the magnification of the lens increases, the observed length becomes short and the resolution for depth of the surface increases as the resolution for distance increases. The maximum depth, namely the distance between the top and the bottom of the trace, is almost constant. More detailed surface topology can be distinguished with a lens having higher magnification. In both static and fatigue fractured surfaces for all magnifications, the relationship between the number of squares, $N(r)$ and the side length, r can be represented by a straight line having a negative slope in the log–log scaled figures.[2]

Fig. 6 shows the variation of fractal dimension, D and $\log C$ (in Eq. (2)) with respect to lens magnification for

[1] When the object lenses were changed, we paid a lot of attention not to move the specimen. Even so, the observed location became slightly different when we changed the object lenses. < /FTN > 1.

[2] The lower limit of 'r' depends on the resolution of the surface trace. When r is shorter than the resolution of the microscope in either direction, the surface trace is regarded as a straight line and the slope of the $N(r) - r$ curve approaches ' -1'. Therefore, a meaningful fractal dimension cannot be estimated if shorter lengths for r than the limitation are included in the $N(r) - r$ curve. When we use the $\times 10$ object lens, the resolution in the longitudinal direction is 0.5 μm and r is limited to higher than 0.5 μm even if the resolution in the vertical direction is higher than 0.5 μm.

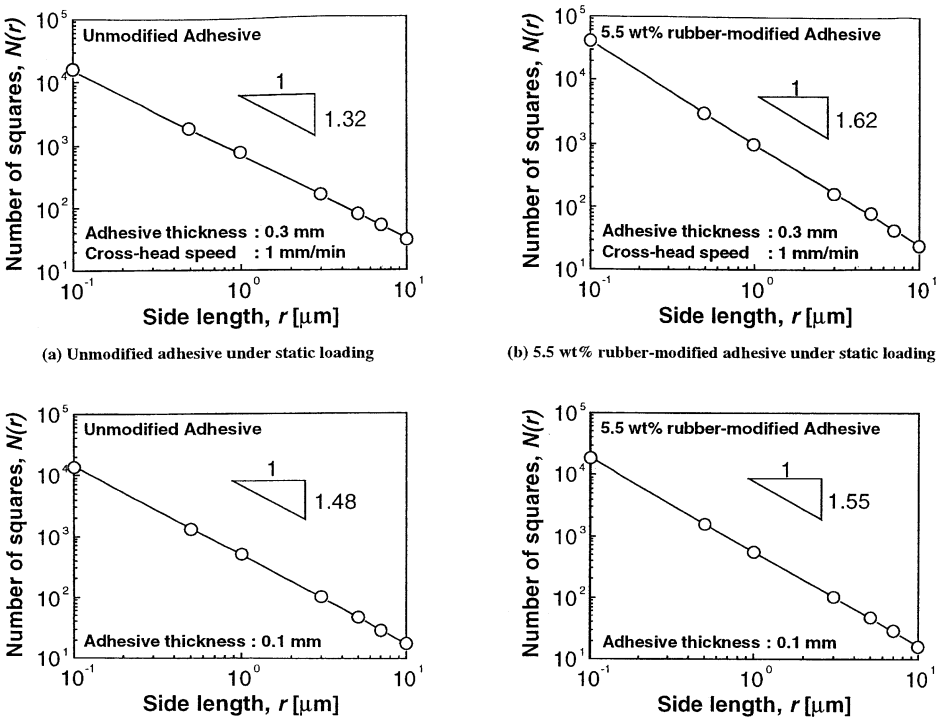

Fig. 4. Relationship between the number of squares $N(r)$ and the side length r for fracture surfaces. (Unmodified and 5.5 wt% rubber-modified adhesives).

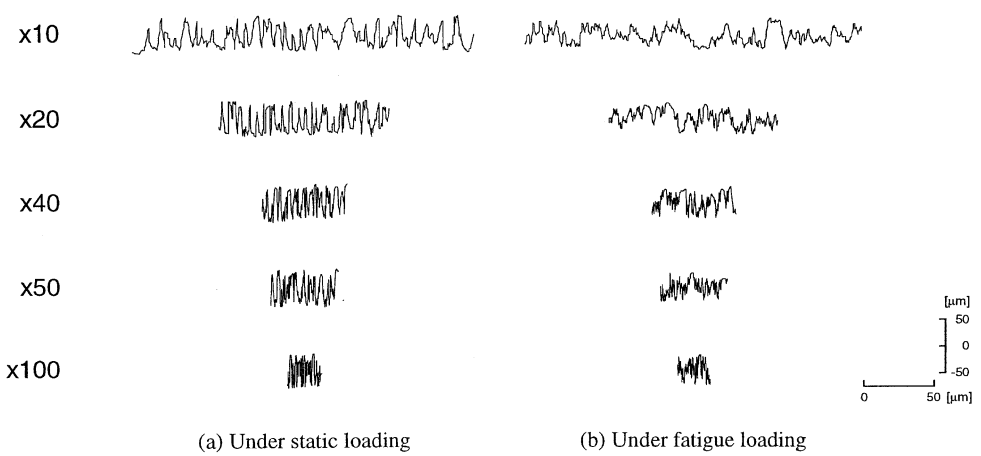

Fig. 5. Surface traces of static and fatigue fracture surfaces for 5.5 wt% rubber-modified adhesive using various object lenses.

both static and fatigue fractured surfaces. For the static fractured surface, D is almost constant although $\log C$ decreases with increasing magnification. For both static and fatigue fractured surfaces, $\log C$ decreases with increasing magnification. D changes slightly at a range of $\times 10$ to $\times 40$. At this range, D increases with increasing magnification. However, D is almost constant for the $\times 50$ and $\times 100$ object lenses. The reason why D changes for fatigue fractured surface due to the object lens magnification must be related to the crack growth rate. As previously mentioned, the energy release rate is not constant regardless of crack length from the loading point for the DCB specimens under cyclic loading at a constant amplitude. Therefore, the crack growth rate is also not constant. When a wide range of fatigue fractured surface is observed for estimating the fractal dimension, it must be difficult to neglect the change in crack growth rate within this range. Thus, both aspects for cracks whose growth rates are slow and fast are involved in the observed failure surface. Consequently, the observed value of D changes due to the observed distance, although the reason why D decreases slightly by increasing

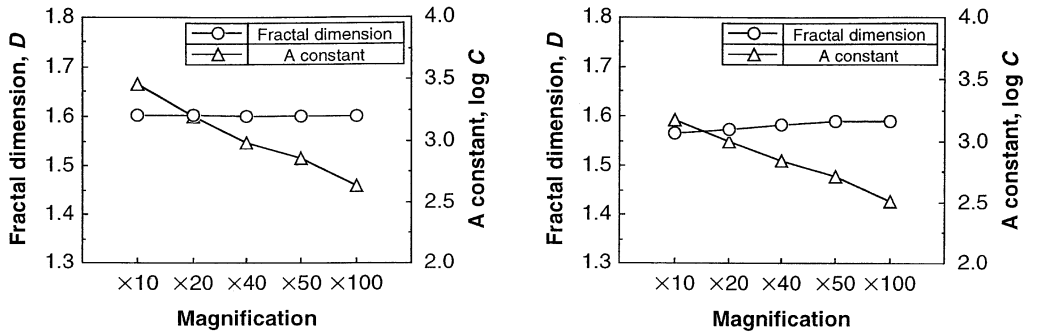

(a) Under static loading (b) Under fatigue loading

Fig. 6. Effect of magnification on the fractal dimension D and a constant C.

the observed distance is not clear. Fig. 7 shows the variation of fractal dimension, D and log C (in Equation (2)) with respect to the number of data (200, 300, 400, 500, 600, 700, 800, 900) for the static fractured surface while the $\times 50$ lens was used. D is almost constant, but log C increases with increasing the number of data. It is found from Figs 6 and 7 that log C (in Eq. (2)) depends on the observed distance (magnification) and the number of data. Based on the above results, we concluded that the $\times 50$ object lens is suitable for tracing the surface topology. We also concluded that the fractal dimension, D should be used as an indicator which can quantitatively characterize the fractured surfaces since the fractal dimension is little affected by both the observed distance and the number of data.

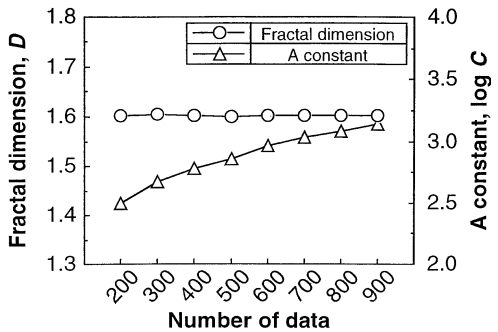

Fig. 7. Effect of number of data on the fractal dimension D and a constant C.

In the mathematical sense, the fractal dimension represents the degree of self-similarity of a curve as can be seen in the von Koch snow-flake curve [14,15]. The fractal dimension of fractured surfaces used in this study is considered as an indicator representing the geometric complexity. It should not be regarded as a parameter representing the degree of the self-similarity[3] Namely, the fractal dimension used in the present work should be a self-affine fractal rather than a self-similar fractal. Here, the self-affine fractal is only self-similar when scaled in one direction [16,17]. 'Self-affine' defines a characteristic in which the objects do not change with different scale of enlargement in one direction [17,18]. The box counting method used for estimating the observed fractal dimension is based on the self-similar concept [16,17]. Therefore, strictly speaking, the usage of the box counting method might cause some problems for estimating the observed fractal dimension of fractured surfaces. However, Figs. 6 and 7 confirm that there are a few problems in practical cases where in the box counting method is used.

There must exist upper and lower limits for the adaptation of Eq. (1) in practical cases. The lower limit of 'r' depends on the resolution of the surface trace as mentioned before in the foot note. The upper limit is an observed length. In this case, the surface trace is presumed to have pseudo-self-similarity within a range where the trace was examined. An infinite trace cannot be measured. Although such limitations exist, the fractal dimension must be effective to characterize the complex geometry of fractured surfaces as long as conditions such as resolution, distance, and the number of data do not change. Similar discussions on the applicability of fractals for surface characterization of metals can be found elsewhere [18–22]. Previously, the fractal dimension was examined from the physical point of view using linear finite element analysis [12]. According to the relationship between the model fractured surface and the fractal dimension (see Fig. 8), the fractal dimension of a fractured surface can be related to the roughness of the surface. As the surface becomes more complex, i.e. rougher, the fractal dimension of the fracture surface increases.

[3]It is also deduced that the fracture process of adhesively bonded joints has a self-similarity. When we observe the failure phenomena of adhesives, the fracture occurs from a microscopic level (damage/yielding) to a macroscopic level (crack) through a mesoscopic state.

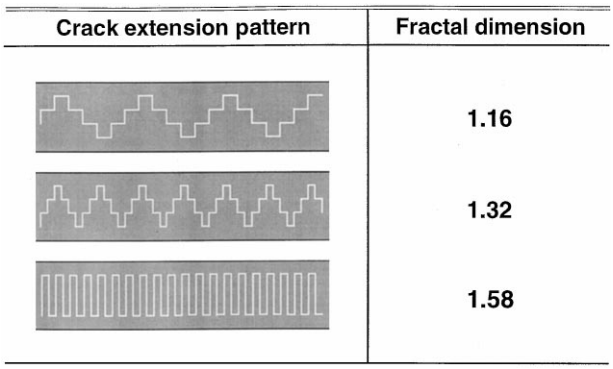

Fig. 8. Model fracture surfaces and their fractal dimensions.

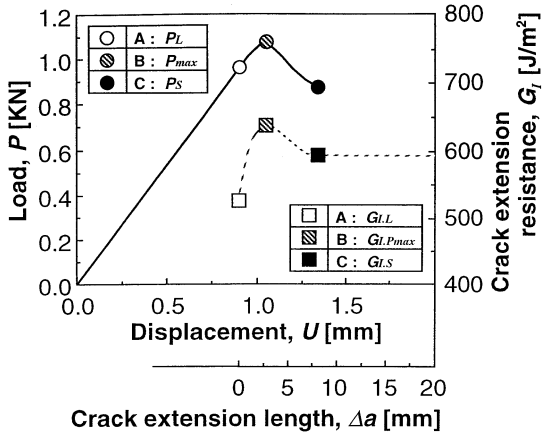

Fig. 9. Load P – displacement U curve and variation of crack extension resistance G_I with respect to crack extension length Δa for 5.5 wt% rubber-modified adhesive. (adhesive thickness = 0.3 min, cross-head speed = 1 mm/min).

We will discuss the effects of rubber modification and adhesive thickness on the static and fatigue fractured surfaces using the fractal dimension below.

3.1. The effects of rubber modification, adhesive thickness and cross-head speed on the static fractured surfaces

Fig. 9 shows the load-displacement curve for 5.5 wt% rubber modified adhesive ($t = 0.3$ mm, $v = 1.0$ mm min^{-1}). The change in crack extension resistance with respect to crack extension length, i.e. R-curve, is also given in the figure [23]. The load increases linearly from zero to Point A. The crack extension resistance at Point A is designated as G_I. Then, the curve becomes non-linear. The load becomes a maximum at Point B. At Point B, the crack extension resistance is designated as $G_{I.Pmax}$ since the load is a maximum. $G_{I.S}$ represents the crack extension resistance at Point C because it changes little with an increase in crack length and the crack grows stably. In the present study, we focus on $G_{I.Pmax}$ among the three crack extension resistances and the R-curve in the fractal analysis.

Fig. 10 shows the variation of fractal dimension and $G_{I.Pmax}$ with respect to rubber content for three types of epoxy adhesives (at conditions of $t = 0.3$ mm and $v = 1.0$ mm min^{-1}). Fig. 11 also shows the variation of fractal dimension and crack extension resistance with respect to crack extension length for three adhesives (at the same conditions as in Fig. 10). In these figures, it is found that the fractal dimension as well as the crack extension resistance becomes high with increasing rubber content. In other words, the fractured surface of epoxy adhesives becomes complex with increasing rubber content.

Fig. 12 shows the relationship between the crack extension resistance and the fractal dimension for three epoxy adhesives, where the data were estimated from Fig. 11. The following equation gives the relationship between the crack extension resistance, G_I (including $G_{I.L}$, $G_{I.Pmax}$,

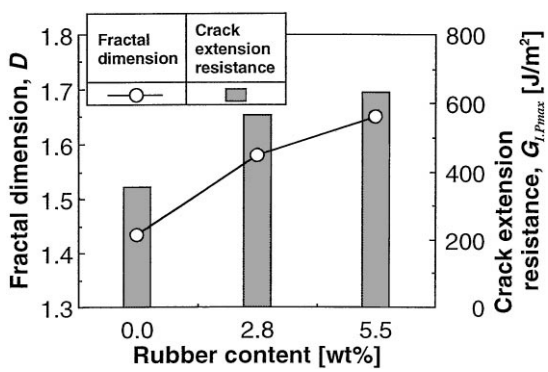

Fig. 10. Effect of rubber content on the fractal dimension D and $G_{I.Pmax}$. (adhesive thickness = 0.3 mm, cross-head speed = 1 mm/min).

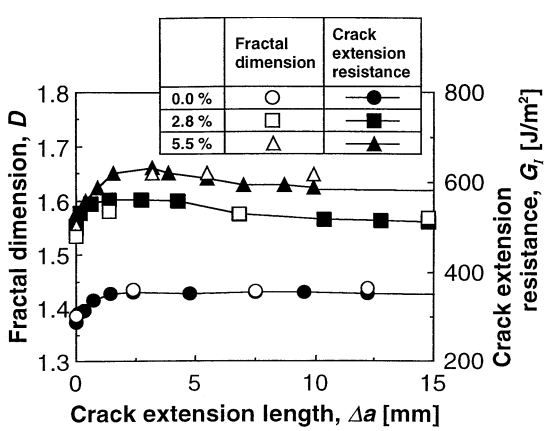

Fig. 11. Variations of the fractal dimension D and crack extension resistance G_I with respect to crack length Δa. (adhesive thickness = 0.3 mm, cross-head speed = 1 mm/min).

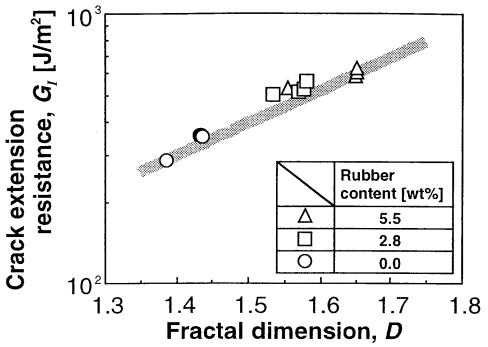

Fig. 12. Relationship between the fractal dimension D and crack extension resistance G_I. (adhesive thickness = 0.3 mm, cross-head speed = 1 mm/min).

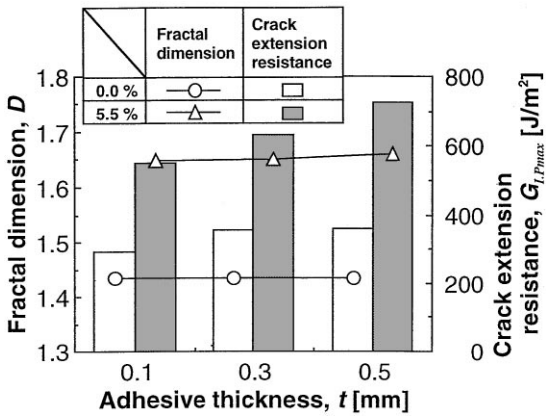

Fig. 13. Effect of cross-head speed t on the fractal dimension D and $G_{I,Pmax}$. (cross-head speed = 1 mm/min).

and $G_{I,S}$) and the fractal dimension, D:

$$\log G_I = \alpha_1 \cdot D + \beta_1 \Lambda \quad (3)$$

where α_1 and β_1 are experimental constants. The fractal dimension of the static fractured surfaces can evaluate the static crack growth properties for both unmodified and rubber-modified epoxy adhesives. As the $D - G_I$ relation can be represented by Eq. (3), we can estimate the crack extension resistance, G_I from the fractal dimension, D for an arbitrary position if the adhesive thickness and the cross-head speed are given. It is estimated from either Eq. (3) or Fig. 12 that a flat surface (with a fractal dimension of 1.0) can be created at about 100 J/m^2 energy when the adhesive thickness is 0.3 mm and the cross-head speed is 1.0 mm min^{-1}. This estimation has not been confirmed by the experiment since all the adhesives failed cohesively under static loading. However, it is interesting that interfacial failure begins at about $\Delta G_I = 100$ J/m^2 under cyclic loading, although this might just be a coincidence.

Fig. 13 shows the variation of fractal dimension and $G_{I,Pmax}$ with respect to adhesive thickness for unmodified and 5.5 wt% rubber-modified adhesives ($v = 1.0$ mm min^{-1}). For the unmodified adhesive, the fractal dimension is not affected by adhesive thickness although $G_{I,Pmax}$ appreciably increases when the adhesive thickness varies from $t = 0.1$ mm to 0.3 and 0.5 mm. On the other hand, for the 5.5 wt% rubber-modified adhesive, $G_{I,Pmax}$ increases linearly and significantly when the adhesive thickness varies from $t = 0.1$ to 0.5 mm. An increase in the fractal dimension is distinguishable, but, it should be noted that the increase is very small.

Fig. 14 shows the variation of fractal dimension and $G_{I,Pmax}$ with respect to cross-head speed for unmodified and 5.5 wt% rubber-modified adhesives ($t = 0.3$ mm). For the unmodified adhesive, the fractal dimension and $G_{I,Pmax}$ are not affected by cross-head speed. For the 5.5 wt% rubber-modified adhesive, the fractal dimension is also not affected by cross-head speed as well although

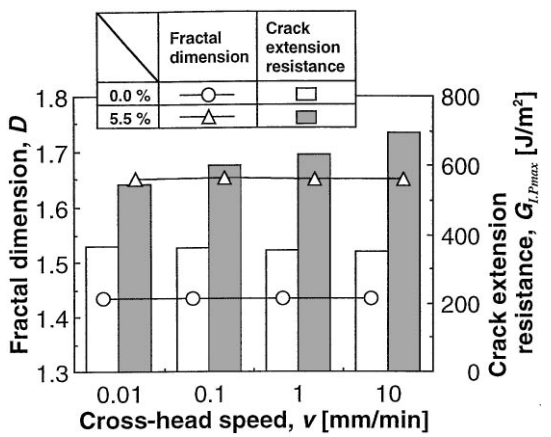

Fig. 14. Effect of cross-head speed v on the fractal dimension D and $G_{I,Pmax}$. (adhesive thickness = 0.3 mm).

$G_{I,Pmax}$ increases linearly when the cross-head speed varies from $v = 0.01$ to 10 mm min^{-1}.

Creating a complex surface means the crack propagates in a zig-zag fashion; the true surface area increases. In the present study, the projected area of the fracture surface is used for G_I estimation, and it is not the true area. The true area (i.e. the actual path between two locations) increases due to crack deflection, even if the projected area (i.e. the straight distance) is constant. Therefore, it is considered that the increase of fractal dimension could explain the increase of the observed crack extension resistance due to an increase of true fractured surface. However, it is known that the surface energy of polymers is very small. The inherent fracture toughness is 1000–10 000 times larger than the energy estimated by the surface energy [24,25]. Based on the above fact, we should recognize that the increase in fractal dimension cannot easily explain the large increase of the crack extension resistance in Fig. 10 and 11,

although an increase of fractal dimension indicates an increase of the true area (i.e. the actual path between two locations) due to crack deflection.

Generally, it is considered that an increase of crack extension resistance, for example fracture toughness, of ductile materials is due to an increase of plastic deformation zones at and near a crack tip [7,24,25]. For epoxy adhesives, the yield stress is lowered by including sub-micron spheres of rubber due to stress concentration around the rubber particles. In addition to plastic deformation, microscopic damage such as sub-micron cracks and delamination must occur around the particles here and there after yielding occurs. Strain at fracture also increases, and strain hardening becomes small. Therefore, a larger plastic deformation and microscopically damaged zone than that for the unmodified adhesive must be formed ahead of the crack due to early yielding of the resin around the rubber particles for rubber-modified adhesives. Plastic yielding grows and micro-scopic damage accumulates at wide areas on both sides of the crack. The rubber (CNBR) particles are so tiny (70–200 nm in diameter) that the strong bridging effect of rubber particles is unexpected for pinning the crack, which is often referred for explaining the toughening mechanisms of rubber modified adhesives and polymers (for example, CTBN modified epoxies [7,26]. The direct crack deflection effect of rubber particles is also less expected because no rubber spheres have been distinguished in the fracture surface and the average depth of the fracture surface is much greater than the mean diameter of the CNBR particles. On the other hand, when CTBN modification is applied to an epoxy adhesive, relatively large rubber spheres and dimples around 2–5 μm in diameter are usually found in the fracture surface of the adhesive [7,26]. In this case, we may say that there exists both direct crack pinning and deflection effects.

When a large zone of plastic yielding and damage has been previously formed ahead of the crack and then the crack propagates into it, the fracture surface must become more complex in correspondence with the degree of plastic deformation/damage and the size of the yielding/damaged zone. The microscopic bridging, crack pinning, and deflection effects may promote the failure surface to be self-affine. An increase of crack extension resistance could be explained by the expansion of the yielding/damaged zone, and also an increase of fractal dimension could be explained by the crack propagating in the plastic/damaged zone previously formed, as shown in Fig. 15. Thus, when a crack propagates into the adhesive layer, plastic zones are formed in the resin, perpendicular to the direction of macro-crack growth. In such a failure which occurs as the result of crack growth with plastic deformation and microscopic damage at a crack tip, the fracture surface becomes more complex in correspondence with the degree of plastic deformation/damage

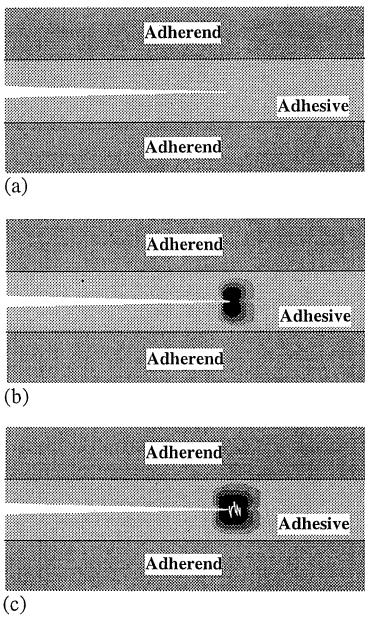

Fig. 15. Schmatic illustrations of plastic deformation and microscopic damage at a crack tip and crack growth: (a) Before loading; (b) Plastic yielding/damaged zone is expanding in adhesive layer; (c) Crack growing into the plastic yielding/damaged zone; previously formed.

and the size of the yielding/damaged zone. Since the fractal dimension of fractured surfaces can be an indicator representing the degree of plastic deformation/damage and the size of the yielding/damaged zone caused by crack propagation, it is related to the fracture toughness of adhesive joints to some extent. Thus, an increase in fractal dimension means not only an increase of true area due to crack deflection, but also an increase in the degree of plastic deformation/damage and in the size of the yielding/damaged zone.

The fractal dimension does not change with variation of adhesive thickness although the crack extension resistance changes with respect to adhesive thickness, as shown in Fig. 13. There must be a limitation for the correspondence of fractal dimension to the size of yielding/damaged zone. It is rational to suppose that the crack in the adhesive layer deflects and grows within a narrow band as shown in Fig. 16 even if plastic yielding and microscopic damage in the adhesive layer is wide spread far away from the crack surface. Figure 16 (a) is different from Fig. 16 (b) in the size of the yielding/damaged zone. The fractal dimensions of both fractured surfaces are almost the same, although the crack extension resistances are different due to the difference in the size of the yielding/damaged zone. The zone which can be evaluated by the fractal dimension is a distance of an arrow in Fig. 16. For both unmodified and rubber-modified adhesives, the change in $G_{\mathrm{I.Pmax}}$ with respect to adhesive thickness is caused by the difference in the expansion

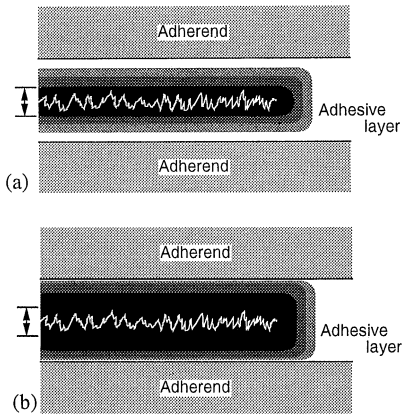

Fig. 16. Schematic illustrations of plastic deformation/damaged zones: (a) Plastic deformation zone is narrow; (b) Plastic deformation zone is wide.

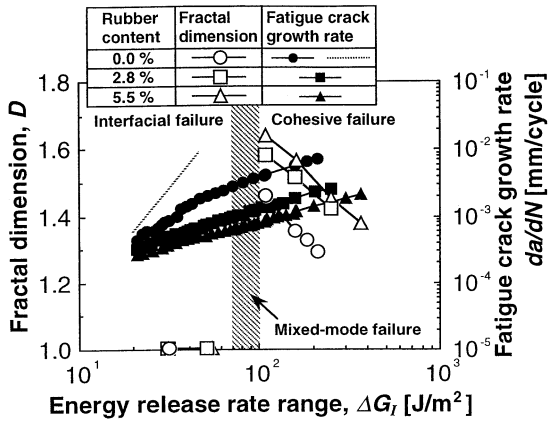

Fig. 17. Effect of rubber content on fractal dimension D and fatigue crack growth behavior (Unmodified, 2.8 and 5.5 wt% rubber-modified adhesives, adhesive thickness = 0.1 mm).

of plastic deformation because the fractured surface topology is not affected by the adhesive thickness. The plastic deformation and microscopic damage accumulation for the adhesive in the thickness direction at a crack tip is restricted by the adherends when the adhesive thickness becomes thin. Therefore, $G_{\mathrm{I.Pmax}}$ for a thin adhesive layer becomes smaller than that for a thick adhesive layer because the energy absorption which is caused by the plastic deformation and microscopic damage near a crack tip becomes small even if the crack propagates in the center of the adhesive layer.

The fractal dimension does not change with respect to cross-head speed, as shown in Fig. 14. An appreciable change in failure mode or failure mechanism is not found when the cross-head speed changes. Therefore, it is supposed that the change of $G_{\mathrm{I.Pmax}}$ with respect to cross-head speed as well as adhesive thickness, is mainly caused by the difference in the expansion of plastic deformation in addition to an increase of energy absorption given by the area below the stress-strain curve due to the strain rate effect (in other words, visco-plastic work).

3.2. The effects of rubber modification and adhesive thickness on the fatigue fractured surfaces

Fatigue crack growth properties can be represented by the relationship between fatigue crack growth rate, $\mathrm{d}a/\mathrm{d}N$ and energy release rate range, ΔG_{I} [27,28]. Fig. 17 shows variations of fractal dimension and fatigue crack growth rate, $\mathrm{d}a/\mathrm{d}N$ with respect to energy release rate range, at the nominal bondline thickness ($t = 0.1$ mm). We also examined the crack growth under other conditions according to the same procedure. The experimental results of all the adhesives are given below:

(1) When ΔG_{I} is lower than 70 J/m^2, the fractal dimension of the fractured surfaces is almost 1.

(2) When ΔG_{I} is greater than 100 J/m^2, the fractal dimension of the fractured surfaces decreased with an increase in ΔG_{I}.

When the fractal dimension of the fractured surfaces is almost 1, the specimens failed in an interfacial manner. At a range of $\Delta G_{\mathrm{I}} = 70$–100 J/m^2, the specimens failed in mixed interfacial-cohesive manner, as shown in Fig. 2b. In this range, with an increase in ΔG_{I}, cohesive failure occurred partially in the center of the adherend and gradually spread over the width direction of the specimen. When ΔG_{I} is larger than 100 J/m^2, the specimens failed cohesively all over the width direction.

Over 20 J/m^2 of ΔG_{I}, the relationship between $\mathrm{d}a/\mathrm{d}N$ and ΔG_{I}, follows the Paris' law [27] as shown in Fig. 17. Even at the range where the Paris' law is applicable, the failure modes change into three types; interfacial, mixed interfacial-cohesive and cohesive failure. In other words, even if the fatigue crack propagates from interfacial failure to cohesive failure, the data of these adhesives does not deviate from the Paris' law or a linear part of the plot on a log–log scale,

$$\frac{\mathrm{d}a}{\mathrm{d}N} = C(\Delta G_{\mathrm{I}})^m, \tag{4}$$

where m and C are experimental constants.

For the same ΔG_{I}, $\mathrm{d}a/\mathrm{d}N$ decreased with increasing rubber content. The fatigue crack growth resistance increased due to rubber modifications at this range as well in the same way as the static crack growth resistance increased. For the same ΔG_{I} (but ΔG_{I} is greater than 100 J/m^2), the fractal dimension of the fractured surface usually becomes large with increasing rubber content.

Fig. 18 shows the variations of D and $\mathrm{d}a/\mathrm{d}N$ with respect to the energy release rate ΔG_{I} for the 5.5 wt% CNBR modified adhesive. Adhesive thickness has little

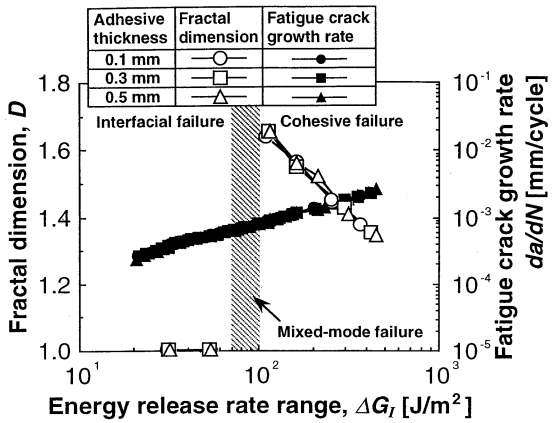

Fig. 18. Effect of adhesive thickness t on fractal dimension D and fatigue crack growth behavior (5.5 wt% rubber-modified adhesive).

effect as the fractal dimension, on the $da/dN - \Delta G_I$ relationship. This coincidence indicates that the failure process in the adhesive layer does not change due to adhesive thickness under cyclic loading. Thus, it is considered that the difference of the size of the yielding/damaged zone formed ahead of the fatigue cracks is small in comparison with the adhesive thickness, since the applied energy release rate is low. Therefore, the $da/dN - \Delta G_I$ relationship is insensitive to adhesive thickness. It has been known that the static crack extension resistance of toughened epoxy adhesives increases with increasing adhesive thickness [23,27]. We previously indicated in this paper that the static crack extension resistance of 5.5 wt% rubber-modified adhesive increased with increasing adhesive thickness although the fractal dimension of the fractured surfaces did not change due to the variation of adhesive thickness (see Fig. 13). A summary of the effect of adhesive thickness on crack growth resistance is given in Table 1.

Probably, one may expect that the fractal dimensions of fractured surfaces under cyclic loading are lower than those under static loading since the applied maximum energy release rate under cyclic loading is lower than that under static loading. However, it must be noted that the fractal dimensions of fractured surfaces under cyclic loading are higher than those under static loading if one looks at Figs. 10–14, 17 and 18. This inconsistency may be resolved by the later discussion. That is, the fractal dimension reflects not only the energy release rate but also the fatigue crack growth rate.

Fig. 19 shows the relationship between the energy release rate range and the fractal dimension ($\Delta G_I > 100$ J/m^2) for unmodified and 5.5 wt% CNBR modified adhesives in the case of cohesive failure. There must exist a certain relationship between the energy release rate range and the fractal dimension. A relationship is given by the following equation between the logarithmic energy release rate range, $\log \Delta G_I$ and the fractal dimension.

$$\log \Delta G_I = \alpha_2 \cdot D + \beta_2, \quad (5)$$

where α_2 and β_2 are experimental constants. Under static loading, G_I increased with an increase in fractal dimension; however, ΔG_I decreased with an increase in fractal dimension under cyclic loading. The $D - \Delta G_I$ relationship is affected by rubber content under cyclic loading. However the D-G_{IC} relationship is not affected by rubber content under static loading. α_2 and β_2 for the unmodified adhesive are different from those for the rubber-modified adhesives under cyclic loading. When adhesives have the same rubber content, the fractal dimension of fatigue fractured surfaces is related to the energy release rate range by Eq. (5). In this case, the fractal dimension is an effective parameter for characterising the fatigue crack growth properties. However, if we do not know the rubber content, the range of the energy release rate at the observed point cannot be estimated by the fractal dimension of the fractured surface. Considering the difference of rubber content, the D-ΔG_I relationship is not enough to evaluate the fatigue crack growth properties.

From Figs. 17 and 18, the existence of a strong correlation between the fractal dimension and the fatigue crack growth rate for all adhesives can be expected. Both da/dN and the fractal dimension decrease with an increase in ΔG_I. A fractured surface corresponding to the loading frequency was formed under cyclic loading.

Table 1
Effect of adhesive thickness t on crack growth resistance and the fractal dimension D under static and fatigue loadings

	Crack extension resistance, G_I / Fracture tougness, G_{IC} (static) → (fatigue) / $da/dN - \Delta G_I$ relation	Fractal dimension, D
Static	◎ (Significant)	× (Little)
Fatigue	× (Little)	× (Little)

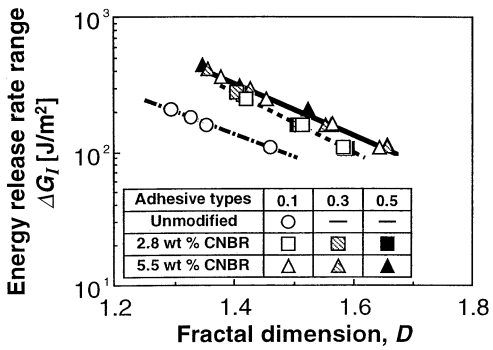

Fig. 19. Relation between energy release rate range ΔG_I and fractal dimension D.

Therefore, we can suppose that the fatigue crack growth rate, which corresponds to the frequency of fatigue crack growth, is strongly related to the fractal dimension. Fig. 20 shows two fractured surface models in order to focus the frequency of fatigue crack growth. Model surface (1) is on the left-hand side and model surface (2) is on the right-hand side. In (1) and (2), the basic surface topology is different. Synthetic surface traces (b)–(e) were generated as follows. (A) is the original fractured surface trace. while (B) is a synthetic surface trace based on trace (A). At first, the length of trace (A) is scaled down by half ($\frac{1}{2}$) without changing its magnitude. Then, a new trace is obtained whose total length is a half of the original surface trace (A). Next, trace (B) is synthesized by joining two of these new traces in series. (C) is also synthesized according to the same procedure while trace (A) is scaled

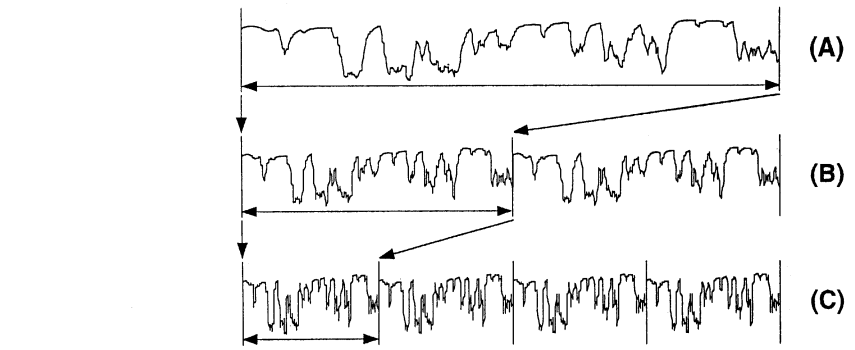

Model surface (1)	Ratio $f^*(=f/f_0)$	Fractal dimension D		Model surface (2)	Ratio $f^*(=f/f_0)$	Fractal dimension D
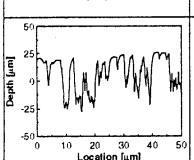	1	1.512	(a)	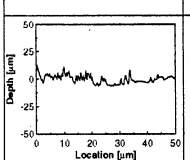	1	1.451
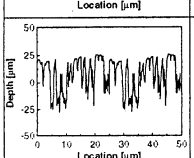	0.5	1.557	(b)	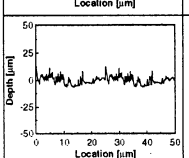	0.5	1.479
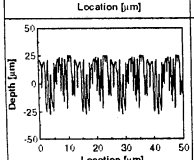	0.25	1.593	(c)	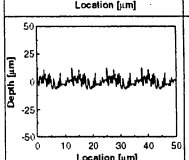	0.25	1.497
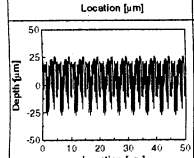	0.1	1.647	(d)	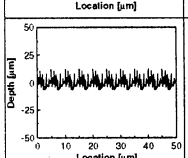	0.1	1.539
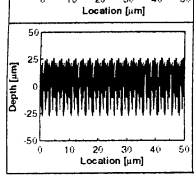	0.05	1.695	(e)	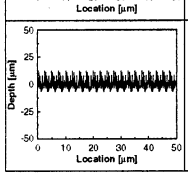	0.05	1.552

Fig. 20. Synthetic surface traces and their fractal dimensions.

down by a quarter ($\frac{1}{4}$) in the length-wise direction. Fig. 20 b–e are synthesized by the same procedure as for trace (B) and (C). (i.e. trace (a) is firstly scaled down by sizes of $\frac{1}{2}$, $\frac{1}{4}$, $\frac{1}{10}$, $\frac{1}{20}$ to create basic traces. Then, they are bonded together as many times as the total length is equal to the original length of trace (a), respectively). In Fig. 20 are shown the calculated frequency ratio, f^* based on trace (a), and the fractal dimension. A linear relationship between the logarithmic frequency ratio ($\log f^*$) and the fractal dimension can be seen in Fig. 21. The fractal dimension decreases with increasing f^*. From this figure, it appears that a strong correlation exists between the frequency of fatigue crack growth, i.e. the fatigue crack growth rate, and the fractal dimension. A relationship is given by the following equation between the frequency ratio and the fractal dimension:

$$\log f^* = \alpha_3 \cdot D + \beta_3, \tag{6}$$

where α_3 and β_3 are constants.

Fig. 22 shows the relation between the fatigue crack growth rate and the fractal dimension for the unmodified and 5.5 wt% CNBR modified adhesives when cohesive failure occurs ($\Delta G_I > 100\ J/m^2$). A relationship is given by the following equation between the logarithmic fatigue crack growth rate ($\log da/dN$) and the fractal dimension:

$$\log \frac{da}{dN} = \alpha_4 \cdot D + \beta_4, \tag{7}$$

where α_4 and β_4 are experimental constants. From Eq. (7), the fatigue crack growth rate can be related to the fractal dimension as previously expected. For many metals, striations which have been created by cyclic crack growth are clearly in evidence for fatigue-fracture under cyclic loading [29,30]. The fatigue crack growth process could be retraced when the striations were found in the fractured surface. However, in adhesives containing many microinclusions, striations are not clearly identified. It is difficult to retrace the fatigue crack growth process from observation of the surface. If the fractal dimension is used in this observation, the fatigue crack growth rate is easily estimated by the fractal dimension. The fractal dimension is therefore useful for analysing the fatigue fractured surfaces.

α_4 and β_4 for the unmodified adhesive are different from those for the rubber-modified adhesives under cyclic loading in that they are dependent on the adhesives used. The D-da/dN relation is not sufficient to evaluate the fatigue crack growth properties (see Fig. 19). As ΔG_I and da/dN are strongly related to the fractal dimension as shown in Eqs. (5) and (7), combining Eqs. (5) and (7) gives the following equations:

$$\log \Delta G_I + \log \frac{da}{dN} = (\alpha_2 + \alpha_4) \cdot D + (\beta_2 + \beta_4), \tag{8}$$

$$\log S = \alpha_5 \cdot D + \beta_5, \tag{9}$$

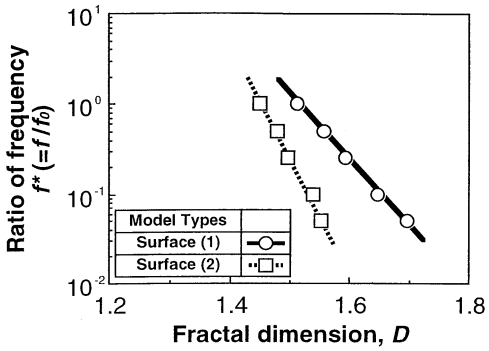

Fig. 21. Relation between frequency ratio f^* and fractal dimension D.

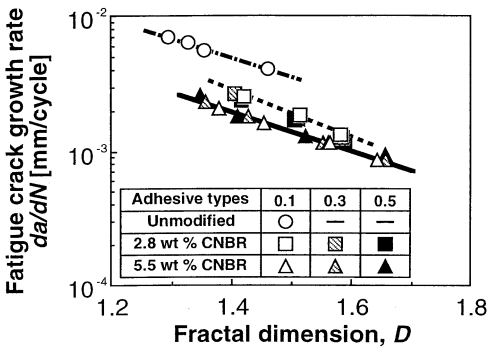

Fig. 22. Relation between fatigue crack growth rate da/dN and fractal dimension D.

where a surface "fatigue working" parameter for the crack, S, and experimental constants, α_5 and β_5 are given by the following equations.

$$S = \frac{da}{dN} \cdot \Delta G_I,$$

$$\alpha_5 = \alpha_2 + \alpha_4,$$

$$\beta_5 = \beta_2 + \beta_4,$$

Fig. 23 shows the relationship between the parameter S and the fractal dimension in the case of cohesive failure ($\Delta G_I > 100\ J/m^2$) for unmodified and 5.5 wt% CNBR modified adhesives (D–S relationship). Regardless of rubber content and adhesive thickness, all the data are plotted on a line. The D–S relationship is insensitive not only to rubber content but also to adhesive thickness. α_5 and β_5 are constant even if the adhesives have different rubber content and adhesive thickness. Corresponding to the fractal dimension of the fractured surface, S can be a universal parameter. Regardless of whether the adhesives contain rubber particles or not, the D–S relationship is effective for evaluating the fatigue crack growth properties of the adhesive based on the same resin.

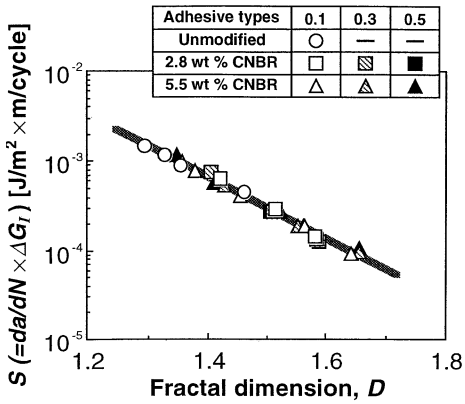

Fig. 23. Relation between a parameter S ($= \mathrm{d}a/\mathrm{d}N \cdot \Delta G_\mathrm{I}$) and fractal dimension D.

In the present study, the $\mathrm{d}a/\mathrm{d}N$-ΔG_I relationship in the case of cohesive failure ($\Delta G_\mathrm{I} > 100\ \mathrm{J/m^2}$) can be represented by the Paris' law as shown in Eq. (4). If we know the material constants, m and C in the Paris law from experiments, we can find the energy release rate range, ΔG_I and the fatigue crack growth rate, $\mathrm{d}a/\mathrm{d}N$ from the fractal dimension, D for the arbitrary position in the center. Even though we do not know m and C of each adhesive, we can find the value of the parameter, S for the position.

4. Conclusions

It was found that the fractured surfaces of epoxy adhesives under mode I static and fatigue loadings have fractal characteristics. We examined the effects of rubber modification, adhesive thickness and cross-head speed on the static and fatigue fractured surfaces of epoxy adhesives using fractals. The following conclusions can be drawn:

Static fractured surfaces and the fractal dimension

(1) The fractal dimension of the fractured surface becomes high due to rubber modification, and the crack extension resistance increases.

(2) The following equation gives the relationship between the observed crack extension resistance, G_I and the fractal dimension, D:

$$\log G_\mathrm{I} = \alpha_1 \cdot D + \beta_1,$$

where α_1 and β_1 are experimental constants.

(3) Regardless of whether the adhesives contain rubber particles, the fractal dimension is not affected by adhesive thickness and cross-head speed, while the crack extension resistance of the unmodified and rubber modified adhesives increases as the adhesive thickness and cross-head speed increase.

Fatigue fractured surfaces and the fractal dimension

(1) The fractal dimension of the fractured surface decreases with an increase in the energy release rate range, ΔG_I.

(2) The fractal dimension becomes high due to rubber modification for the same ΔG_I.

(3) Whether the adhesives contain rubber particles or not, the fractal dimension as well as the $\mathrm{d}a/\mathrm{d}N - \Delta G_\mathrm{I}$ relationship is little affected by adhesive thickness.

(4) The fatigue crack growth rate is well estimated by measuring the fractal dimension of the fracture surface.

(5) A relationship is given by the following equation between a surface "fatigue working" parameter for the crack, S ($= \mathrm{d}a/\mathrm{d}N \cdot \Delta G_\mathrm{I}$) and the fractal dimension for unmodified and rubber-modified adhesives:

$$\log S = \log\left(\frac{\mathrm{d}a}{\mathrm{d}N} \cdot \Delta G_\mathrm{I}\right) = \alpha_5 \cdot D + \beta_5,$$

where α_5 and β_5 are experimental constants.

References

[1] Green DL, Nicholson PS, Embury JD. Fracture of a brittle particulate composite, Part 1 experimental aspects. J Mater Sci 1979;14:1413–20.
[2] Yee AF, Pearson RA, Toughening mechanisms in elastomer-modified epoxies, Part 1 mechanical studies. J Mater Sci 1986;21:2462–74.
[3] Kinloch AJ, Maxwell DL, Young RJ., The fracture of hybrid-particulate composites. J Mater Sci 1985;20:4169–84.
[4] Yee AF, Pearson RA Toughening mechanisms in elastomer-modified epoxies, Part 2: microscopy studies. J Mater Sci 1986;21:2475–88.
[5] Yee AF, Pearson RA Toughening mechanisms in elastomer-modified epoxies, Part 3: the effect of cross-link density. J Mater Sci 1989;24:2571–80.
[6] Garg AC, MY Wing. Failure mechanisms in toughened epoxy resins – A review. Comp Sci Tech 1988;30:179–223.
[7] Kinloch AJ In: 'STRUCTURAL ADHESIVES Developments in Resins and Primers'. Auslerdam: Elsevier, 1986: pp. 127–61.
[8] Bascom WD, Cottington RL, Jones RL, Peyer P. The fracture of epoxy- and elastomer-modified epoxy polymers in bulk and as adhesives. J Appl Poly Sci 1975;19:2545–62.
[9] Hunston DL, Bascom WD, Failure behavior of rubber-toughened epoxies in bulk, adhesive, and composite geometries. Advances in chemistry series 208, Washington DC: Am Chem Soc, 1984:83–99.
[10] *JIS B 0601-1994*. Surface roughness - definitions and designation, 1994.
[11] *ISO 468–1982*. Surface roughness - parameters, their values and general rules for specifying requirements, 1982.
[12] Naito K, Fujii T. Fractals for fractured surfaces of adhesives under static and fatigue loadings. Int J Adhes Adhes. 1995;15(3):123–30.
[13] Nejigaki K. Properties and applications of rubber-toughened epoxy resins. Plast Japan 1992;42(11):139–45.
[14] Takayasu H. Fractals Tokyo, Asakura Shoten. 1986: 1–31, 154–76.
[15] Falconer KJ., The Geometry of Fractal Sets. Cambridge: Cambridge University Press, 1985: 7–10.

[16] Voss RF. In: The science of fractal images. Peitgen H Saupe D, editors. New York: Springer, 1988: 21–69.
[17] Poon CY, Sayles RS, Jones TA. Surface measurement and fractal characterization of naturally fractured rocks., J Phys D 1992; 25:1269–75.
[18] Kurosaki Y, Matsui M, Kitoh T, Takayama T. Fractal analysis of free surface profile of sheet metals under uniaxial tension. Trans Japan Soc Mech Eng 1996; 62, (603): 4107–13.
[19] Talibuddin S, Runt JP. Reliability test of popular fractal techniques applied to small two-dimensional self-affine data sets. J Appl Phys 1994; 76 (6): 5070–8.
[20] Tanaka M. Fractal dimension of the grain boundary fracture in creep-fracture of cobalt-based heat resistant alloys. J Mat Sci 1996;31:3513–3521.
[21] Pande CS, Richards LR, Smith S. Fractal characteristics of fractured surfaces. J Mater Sci Lett 1987;6:295–7.
[22] Mecholsky JJ Jr, Fraeiman S., Relationship between fractal geometry and fractography. J Am Ceram Soc 1991;74:3136–38.
[23] Tsuchida M, Naito K, Fujii T. Effects of CNBR modification on mode I fracture of epoxy adhesives for automotive application. SAE Technical Paper Series, 1994: 950130.
[24] Narisawa I. Fracture toughness of plastics. Tokyo: Siguma Shuppan Publ., 1994: pp 53–79.
[25] Narisawa I. Impact resistance of plastics. Tokyo: Siguma Shuppan Publ., 1994: pp. 117–79.
[26] Hwang JF, Manson JA, Hertzberg RW, Miller GA, Sperling LH Fatigue crack propagation of rubber-toughened epoxies. Poly Eng Sci 1989: 29(20): 1477–87.
[27] Mall S, Ramamurthy G. Effect of bond thickness on fracture and fatigue strength of adhesively bonded composite joints. Int J Adhes Adhes 1989; 9(1): 33–7.
[28] Hayashi S, Naito K, Fujii T. Fatigue fracture characteristics of toughened epoxy adhesives under mode I loading, effects of glass beads and CNBR rubber modification. SAE TECHNICAL PAPER SERIES, 1995: 960 576.
[29] Kitagawa H, Koterazawa R. Fractography. Tokyo: Baifukan, 1977: pp. 1–22.
[30] Komai K. Image processing technique of fracture surface. FATIGUE 90 Proceedings of the Fourth International Conference on Fatigue and Fatigue Thresholds held on 15–20 July in Honolulu Hawaii, 1990: 1963–72.